Received: 19 January 2024 | Revised: 4 March 2024 | Accepted: 31 March 2024

DOI: 10.1002/jrs.6676

RESEARCH ARTICLE

Journal of RAMAN SPECTROSCOPY WILEY

Alteration in the Raman spectra of characteristic rock-forming silicate mixtures due to micrometeorite bombardment

Iris Weber[1] | **Sergey G. Pavlov**[2] | **Ute Böttger**[2] | **Maximilian P. Reitze**[1]

[1]Institut für Planetologie, University Münster, Münster, Germany

[2]Institute of Optical Sensor Systems, Berlin, Germany

Correspondence
Iris Weber, Institut für Planetologie, University Münster, Wilhelm-Klemm-Str. 10, Münster 48149, Germany.
Email: iris.weber@uni-muenster.de

Funding information
Deutsches Zentrum für Luft- und Raumfahrt, Grant/Award Number: 50 QW 1701

Abstract

Innovative techniques are required for the in situ investigation of the surfaces of planetary bodies when landings are planned. Raman spectroscopy turned out as an excellent tool for fast mineralogical analyses on space missions. Contribution from a photoluminescence signal is not unexpected and is likely to be even more pronounced on celestial surfaces with a dilute or absent atmosphere exposed to strong space weathering, for example, micrometeorite bombardment. Such signals were found, for example, in Raman analysis of the probes from sample-return missions. While photoluminescence is generally considered as an accompanying undesired product in the Raman spectral measurement, our studies show that some analytical information can be derived from this signal, and even more, due to the specific correlation of luminescence intensity with space weathering products. Therefore, we investigate the Raman spectra alteration of characteristic rock-forming mineral mixtures (olivine, pyroxene and plagioclase) by micrometeorite bombardment, which is simulated by nanosecond-pulse laser irradiation. The changes in the minerals are strongly dependent on the composition and structure. They range from disappearing changes in the minerals with simple chemistry and structure to complete amorphization of minerals with relatively low melting enthalpy. With Raman spectroscopy, we found out that the photoluminescence signals show resonant or anti-resonant changes to specific mineral phases and amorphization. Furthermore, ablation-induced iron nanoparticles of minerals containing Fe are detectable by Raman spectroscopy due to their alteration into iron oxides. Trapped volatiles in the matrices are analysed due to the formation of the compounds containing them. This broad spectrum of results indicating specific change phenomena due to space weathering can be effectively used for in situ Raman analysis in planetary missions.

KEYWORDS

photoluminescence, simulated micrometeorite bombardment, space missions, space weathering

1 | INTRODUCTION

One of the strategic goals of space missions is to understand the planetary formation and evolution in our Solar System in order to be able to draw conclusions about earlier geochemical processes, for example, on Mars and its moons, Mercury, the Moon and other celestial rocky objects, such as asteroids. Especially, the understanding of processes such as space weathering (SW) caused by high-speed impacts that change the chemical and/or structural composition of planetary surfaces has been significantly enhanced by space missions. Ideally, in situ measurements of the mineralogy and petrology of the rocky surfaces are viable.

In recent years, new instruments, based on both single technique or complementary analytical devices, have been designed in order to achieve these goals. For in situ missions with short-living landers, powerful analytical techniques, such as Raman spectroscopy,[1] came in front due to their analytical capability as a sole technique. Raman spectroscopy requires no sample preparation and is a non-destructive spectroscopy technique suitable for working in a variety of environmental conditions, including different temperatures and pressures in the near-surface atmosphere in vacuum.

There are currently two Raman instruments on the Mars 2020 rover Perseverance: a 532 nm laser pulsed spectrometer in the SuperCam suite and the continuous wave (cw) 248.6 nm laser SHERLOC Raman instrument.[1] These instruments are able to look for signatures of past life and water and examine the composition of the surface, which allows conclusions to be drawn about the formation conditions.

Analogous scientific goals are objectives for the Mars missions ExoMars Rover[2] by ESA and Martian Moons eXploration[3] (MMX) by JAXA to the Martian moons Phobos and Deimos; both with a 532 nm cw Raman laser spectrometer on-board. In contrast to the NASA's rover missions, analytics of these missions relies solely on the data obtained from Raman spectroscopy, making it of large importance. Especially, the Raman instrument (RAX) on MMX will investigate the minerals on the surface of Phobos—as an atmosphere-less body—in situ, in particular to contribute to understanding of the origin and evolution of this Martian moon and the transport and relocation of space debris material around Mars.[4]

With the intention of optimizing the interpretation of the expected in situ data, it is essential in the preparation of such missions to investigate possible analogue materials, including their alteration, in advance,[5–9] because the received in mission Raman spectra have largely to be compared with existing databases on the Earth and extraterrestrial rocks and minerals, respectively.

The surface of bodies without atmosphere in our Solar System is affected by SW that can be triggered by various factors such as heat and pressure-related metamorphism, solar flares and impacts of objects various in sizes. As a product of SW, the so-called regolith is formed on the surface from the existing bed rock through the physical and chemical weathering. This loose and in part coagulated material on the surface of silicate-rich bodies consists mainly of silicate rock-forming minerals, such as olivine, enstatite and feldspar, as well as amorphous glasses.[10] The minerals are altered due to various SW processes[11] that can led to structural and chemical changes in the minerals, such as breaking molecular bonds, amorphization and forming of nanophase iron.[12–15]

In the present laboratory simulation study, the effect of micrometeorite bombardment of solid, silicate-rich surfaces on bodies without atmosphere (e.g., Phobos, Mercury and asteroids) as one activator of SW is investigated with Raman spectroscopy. This SW effect is simulated with an excimer laser impinging the sample surface with short pulses at an energy density of up to ~2 J/cm^2 at low pressure.

In a former Raman SW study,[9] we examined the two silicates, olivine and enstatite, and their mixtures, with the key result that laser irradiation reduced the photoluminescence (PL)-dominated background signal, which is mainly olivine related. The origin of PL detected under 532 nm laser excitation is most likely due to various luminescent impurities in natural crystals, such as rare earth element centres, uranyl groups, aromatic compounds or other lattice defects.[16]

Expectations for the PL properties of extraterrestrial surface soils go in several directions. While the same origins of PL are expected on celestial bodies with atmospheres, strong SW effects on atmosphere-less surfaces are expected to cause a higher density of defects in mineral lattices. On the other hand, a strong surface charge, as known from the Moon, can have other effects on Raman signals (RS) and RS/PL contrasts in in situ Raman spectra. In studies of meteorites compared to analogous terrestrial minerals,[17] it was that reported significantly reduced non-RS contributions in the Raman spectra measured under 532 nm laser excitation. However, the PL properties can be strongly altered under extreme thermal conditions, as they occur when micrometeorites enter the atmosphere: For example, metamorphism of various phases, such as feldspar and enstatite, can lead to the abolition of PL due to melting.[18] The Raman studies of various lunar soils returned from the

Apollo missions did not provide reliable information on the relative PL contribution.[19] Significant background signals were observed in the Raman spectra of particles returned to the asteroid Itokawa by the JAXA Hayabusa mission.[20]

In this work, we present Raman spectroscopic data for olivine and two pyroxenes (enstatite and diopside) mixtures including plagioclase, as another important rock-forming mineral.

The SW produced by simulated laser-induced experiments have already been investigated on various mineral phases using infrared spectroscopy (IR) and scanning and transmission electron microscopy (SEM/TEM) (see Weber et al.[21] and references therein).

However, there are almost no studies that deal with the alteration of the Raman spectra of rock-forming minerals due to micrometeorite bombardment. Even though Brunetto et al.[22] and Matsuoka et al.[23] have dealt with the topic SW, they focus on carbon and its alteration expressed in the D (disordered graphite lattice) and G (graphite-type lattice) bands. And although carbonaceous phases are of high interest due to their occurrence in the Solar System (e.g., on the surface of Phobos or other parent bodies of carbonaceous chondrites), rock-forming silicates, such as olivine, pyroxene and plagioclase, dominate the regolith of atmosphere-less celestial rocky bodies. Therefore, the aim of this work is to study SW on rock-forming minerals using Raman spectroscopy in the context of upcoming space missions.

We present the influence of micrometeorite bombardment simulated with an excimer laser on mineral mixtures containing the silicates olivine (Fo_{91}), enstatite (En_{87}) and diopside ($En_{46}Wo_{50}$)—both pyroxenes—and the low-plagioclase ($An_{51}Ab_{47}$). Forsterite (Fo) and enstatite (En) contents give the amount of Mg in the structural formula of the minerals, wollastonite (Wo) the amount of Ca for pyroxene. Anorthite (An) gives the amount of $CaAl_2Si_2O_8$, and albite (Ab) gives the amount of $NaAlSi_3O_8$ in the composition of the plagioclase sample structural formula of this mineral.

The non-irradiated and irradiated pellets were investigated in the Raman Stokes shift range from 200 to 1,200 cm^{-1}. The most intense spectral feature of olivine is a double peak (DP), caused by the two SiO_4-stretching (ν_1 and ν_3) Raman-active modes, between ~815 and ~860 cm^{-1} for Fe-Mg-olivines.[24] Pyroxene shows the Raman-active vibrational modes between ~220 and ~1,050 cm^{-1}, with prominent Raman shifts between 650 and 700 cm^{-1}—moderate Si-O-Si bending mode—and between 1,000 and 1,050 cm^{-1}—Si-O stretching mode.[25] The most characteristic Raman active modes of plagioclase are in the range from 450 to 520 cm^{-1}, which corresponds to the T–O–T vibrations, with T = (Si, Al) in the four-membered TO_4 tetrahedron rings in a mixed Si-O-Si (Si-O-Al) stretching and bending mode of the SiO_4 and AlO_4 tetrahedral framework.[26,27] In relation to the tetrahedral framework, a distinction can be made between high degree of Al,Si ordering (low plagioclase), resulting in sharper bands and high degree of Al,Si disorder (high plagioclase) resulting in more broader bands. Because of the narrower bands, we used a low plagioclase in our study (cf. Section 2).

Based on these characteristic peak positions, we discriminate between olivine, pyroxene and plagioclase in mixtures.

With this study, we address micrometeorite bombardment as one source of SW retrieved by analysis of Raman spectra of olivine, pyroxene and plagioclase. Such measurements widen the classes of studied rock-forming silicates under such type of SW and can support the thorough interpretation of in situ Raman spectra of current and future space missions.

2 | SAMPLES AND METHODS

2.1 | Samples and preparation

For this study, several natural silicates were selected—a low plagioclase (ID 28/An51Ab47Or2) from Ihosy (Madagascar),[28] an olivine (ID249/Fo91) from the Dreiser Weiher (Germany), an enstatite (ID53/En87) from Bamble (Norway),[9] a diopside (ID22/En46Fs4Wo50) from Otter Lake,[15] Quebec (Canada) and a quartz (ID13)[10] from Mongolia—as expected analogues of rock-forming minerals for most silicate-dominated planetary bodies. Although the minerals are hand-picked, due to the natural nature of the samples, they are not absolutely pure mineral separates. The powder of olivine contained ~8 Vol.% pyroxene as well as phyllosilicates, while the pyroxene itself was serpentinized of up to 10% by volume. The samples are labelled with an identification number (ID) for an unambiguous later identification in the database (http://bc-mertis-pi.uni-muenster.de/); all these samples are additionally used to create a mid-IR database. Chemical analyses of the listed minerals are given in this database also.

After a chemical characterization, the minerals were crushed with a steel mortar, sieved into different grain sizes and then mixed in the assemblage listed in Table 1.

The powdered minerals were mixed with the mean grain size fractions from 63–125 μm, representing a planetary surface texture.[29] Experience from previous studies[9,30] shows suitability of pressed powder samples in contrast to loose powders for laser-induced impact simulation. Containers with loose powders occur to be quickly

TABLE 1 Assemblage of the starting (original) pellets in wt.%

ID	Minerals (wt.%) Olivine (ID249)	Enstatite (ID53)	Diopside (ID22)	Plagioclase (ID28)	Quartz (ID13)
359 smooth plains mix	10	12	19	59	-
360 smooth plains mix	11	24	4	61	-
361 smooth plains mix	100	-	-	-	-
362 high-Mg province mix	49	1	36	11	3
363 high-Mg province mix	63	-	37	-	-

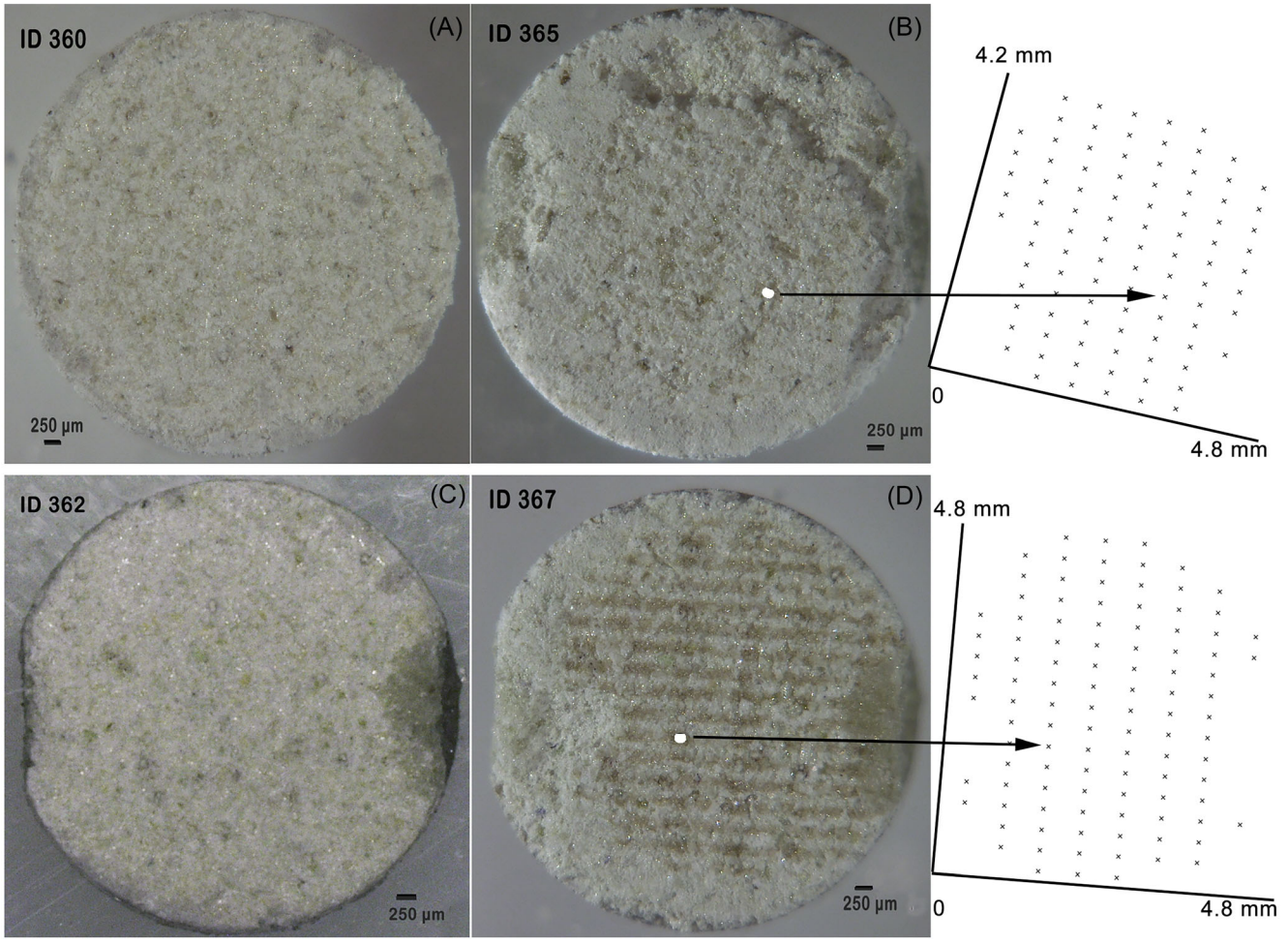

FIGURE 1 Images of the pellet surfaces ID 360 and 362 before (A, C) and after the laser irradiation (ID 365 and 367; B, D) done with a KEYENCE Digital Microscope. The spatial distribution of shots is shown on the right; one example of a shot is given in the microscope image and marked with an arrow.

emptied by laser shots, while the larger volume of pressed pellets remains after irradiation and, therefore, is useful for following up analysis. Although dust-like regolith replicate 'morphologically' rather loose powders than pressed matrices, strong 'sticking' of grains on surfaces of many atmosphere-less celestial bodies due to a large electric charge makes pressed pellets as a good 'physical' analogue. While the Coulomb forces between charged particles are (spatially) short range, they enable a certain mechanical stability, at least for the small size fractions. Furthermore, the surface of moderately pressed pellets is not as dense as within stony bulk (planetary bed rocks) or single crystalline minerals (laboratory analogues), so that we can reproduce a reasonably close to a real regolith structure, which makes them to an ideal counterpart to the regolith of planets or moons without atmosphere.

To obtain mechanically stable pellets, a P/O Weber hydraulic press was used, which was operated for 25 min at about 20 kN. In this process, the individual particles are further crushed by pressing so that the final particle size is between '0' and 125 μm. The compact sample pellet was limited to a diameter of 6 mm and a height of ~3 mm due to the size of the sample holder in the vacuum chamber.[9]

The mixed samples as well as the laser irradiated samples got new IDs (cf. Table 1): IDs: ID359 → 364, ID360 → 365, ID361 → 366, ID362 → 367, ID363 → 368.

2.2 | Methods

The pressed pellets were photographed with a KEYENCE Digital Microscope VHX-500F at the Institut für Planetologie (IfP), Münster, before and after laser irradiation (Figure 1), to track and document the laser shots. Furthermore, we used a JEOL 6610-LV scanning electron microscope (SEM)—operating in a low vacuum mode—to optically detect changes on the sample surfaces after irradiation. Backscattered electron (BSE) images were taken with an acceleration voltage of 20 kV. The composition of the minerals was analysed with a JEOL JXA-8530F Hyperprobe electron probe micro analyser (EPMA) at the Institute of Mineralogy, Münster, before pressing (cf. Weber et al.[9] for more details).

The samples were held in a high-vacuum chamber, simulating planetary bodies without atmosphere, during irradiation and as long as possible after it. While atomic emission from the laser-ablated ejecta in previous simulation studies[31] reveal a residual abundance of ambient atmosphere obviously trapped in the remained cavities between particles in the pressed pellets, its influence on the Raman spectra of silicates is vanishing. The pressure to at least 10^{-4} Pa was achieved with a newly designed Praying Mantis™ high-temperature reaction chamber.[9] The chamber provides an optical access to a sample and is suitable for the use of laser irradiation and directly following analytics (further details can be found in Weber et al.[9,15]).

The micrometeorite bombardment on the pressed pellets was simulated by the excimer laser system (ArF UV laser; wavelength 193 nm) LPX120i (Lambda Physik AG [Coherent Inc. United States]). The UV laser generated 15 ns pulses in a series of three shots per point at a 'starting pressure' in the chamber of 10^{-4} Pa. The energy density was determined between 1.64 and 1.89 J/cm^2 over the whole area with a rectangular 300 × 800 μm^2 laser beam and with an inner laser spot of 140 × 150 μm^2 in focus, which is crucial for the bombardment photon density.[32] The bombardment points were positioned (as 2D maps) in y and in x directions (steps are 300 and 800 μm, respectively) by manually moving the chamber with the sample under the fixed optical direction of a laser beam (Figure 1, right).

Raman measurements were performed with a confocal Raman microscope WITec alpha300R system at DLR, Berlin, with a laser excitation wavelength of 532 nm and pixel resolution of about 4 cm^{-1}. A diagnostic spot size on the pellets of about 1.5 μm was reached with a Nikon 10X objective. In order to replicate the Raman laser intensity for space instrumentation and to reflect conditions of space missions, such as RAX, spectra were taken at 3 mW, which corresponds to 1.7 mW/μm^2 on the sample. In total, 2,500 spectra per sample were acquired over an area of a 1,000 × 1,000 μm^2 field scanned with 50 × 50 points (20 μm step) and an integration time of 2 s per spectrum. This short measurement time per spectrum is sufficient to derive a statistical statement about the natural behaviour of PL from a large number of spectra in a reasonable time, even though it leads to a reduced signal-to-noise ratio. Furthermore, PL signals in the recorded Stokes ranges exhibit broad-band spectra with no specific, discrete-line features and with the shapes that follows roughly the spectral sensitivity of a silicon-based CCD detector. However, the surface roughness of the sample pellets (in the order of the objective Rayleigh length) leads to a variation in the signal-to-noise ratio over the spectra at different locations and makes it necessary to work statistically and with medium focus. But this does not, though, affect the interpretation of the observed minerals' relevant Raman bands. Nevertheless, the variability of the Raman response was controlled with respect to the laser intensity on the sample surface via the intensity of the Rayleigh scattered light, which is not completely suppressed by the filter in the collection optics of the Raman microscope. Typical variations of this signal (standard deviation) are within 2% for the scans of the irradiated samples, with the error bar not exceeding 4 × 10^{-4}. A few strong outliers that occurred in some scans were disregarded in the analysis for both the original and irradiated samples. The broad-band background in the Raman spectra (Figure 3A,C) was removed by the internal software in the spectrometer; the spectra with the reduced background are shown in Figure 3B,D and in Figures 4–6.

3 | RESULTS

The light microscopic images of the non-irradiated and irradiated samples show strong differences (Figure 1). The irradiated pellets, which mainly contain plagioclase only, exhibit evidence of the laser treatment in the form

of a crater-like matrix structure (Figure 1B, ID 365). On the surface of the samples containing mineral phases with moderate iron (such as ID362/367 with about half of olivine), the darkened lines, most probable presenting a production of nanophase iron (np-Fe^0), appear at the positions of laser in the form of dark lines (Figure 1D, ID 367). Figure 1 also shows the good dense laser coverage of the entire pellet surface. The laser spots (irradiation matrix) are illustrated in a sketch on the right-hand side of the light microscope images.

As another result, the further reducing of the mean size in the distribution of the grains minerals due to heating and shock impacts in the pellet is visible in the SEM. Now minerals are present in sizes from less than one μm to ~100 μm (Figure 2A,C). This size distribution is very close to the typical regolith sizes[33] expected on solar system objects without atmosphere.

BSE images of the sample surfaces before and after laser irradiation show a clear response of the minerals to the laser energy. Figure 2 compares the non-irradiated and irradiated samples with the same initial composition. Figure 2B,D is examples of the irradiated surfaces. Although some areas are less affected by the laser when they are not in the irradiation zone, out of the spots (foci) do not experience a full irradiation strength, the large areas of irradiated pellets show extensive melting (especially plagioclase—Figure 2B; ID 365), and when the olivine (Fo91) is dominating in the pellet, the presence of a np-Fe^0 is particularly noticeable (Figure 2D; ID 366). However, a np-Fe^0 is also present in the pyroxene-dominated sample (Enstatite/En and Diopside/Di mostly), but to a lesser extent (see also Weber et al.[15]).

Figure 3 shows typical Raman spectra of the sample IDs 360/365 and IDs 363/368 presenting areas with the

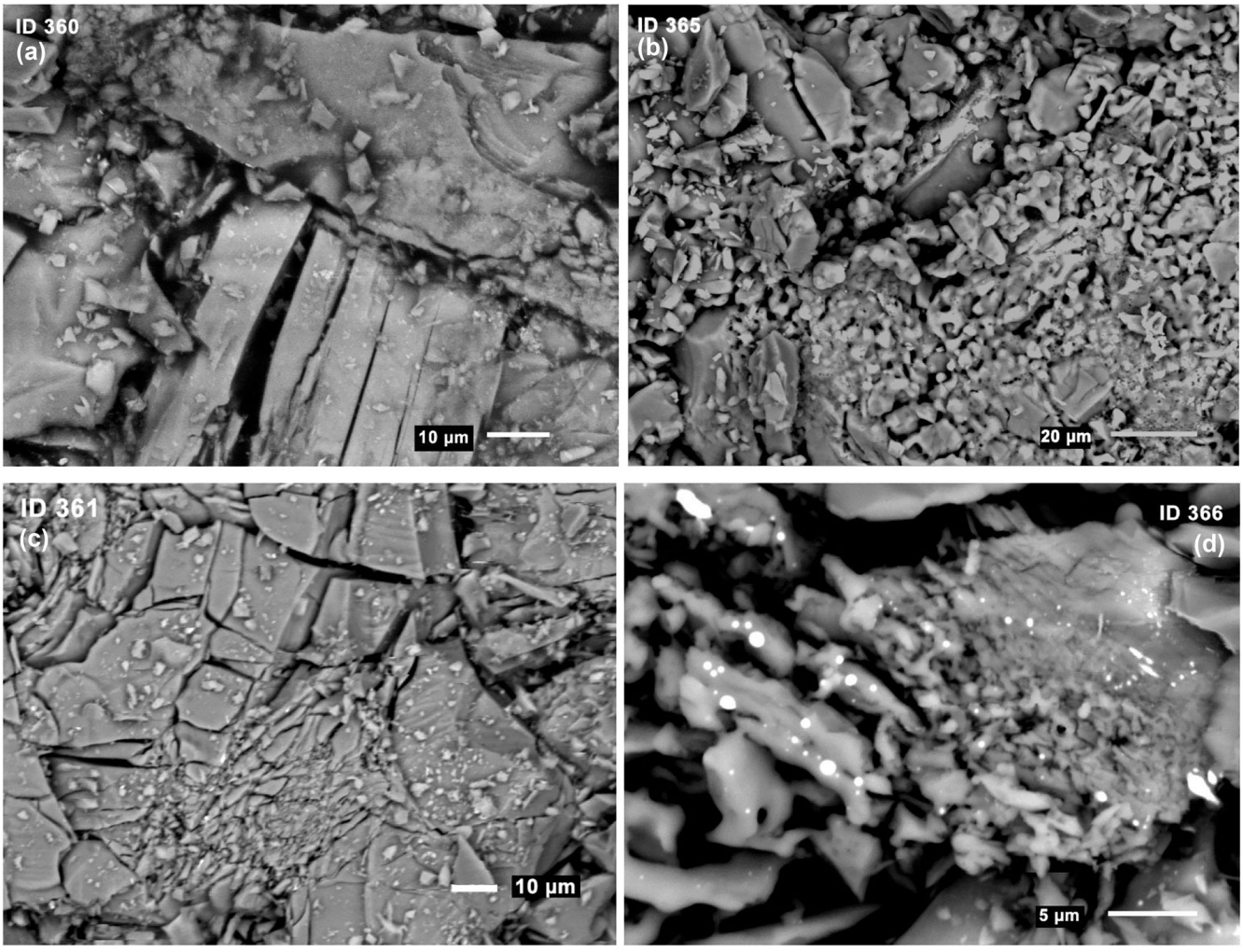

FIGURE 2 BSE images of non-irradiated (A, C) and irradiated (B, D) pellets. (A) ID 360 (plagioclase-rich sample); various grain sizes of the pellets are visible. (B) ID 365 (original ID360). Molten parts of the pellet, mainly plagioclase, including spherules. (C) ID 361 (olivine-rich sample); various grain sizes of the pellets are visible. (D) ID 366 (original ID361). Molten mineral(s) covered with np-Fe^0 particles visible as white globules

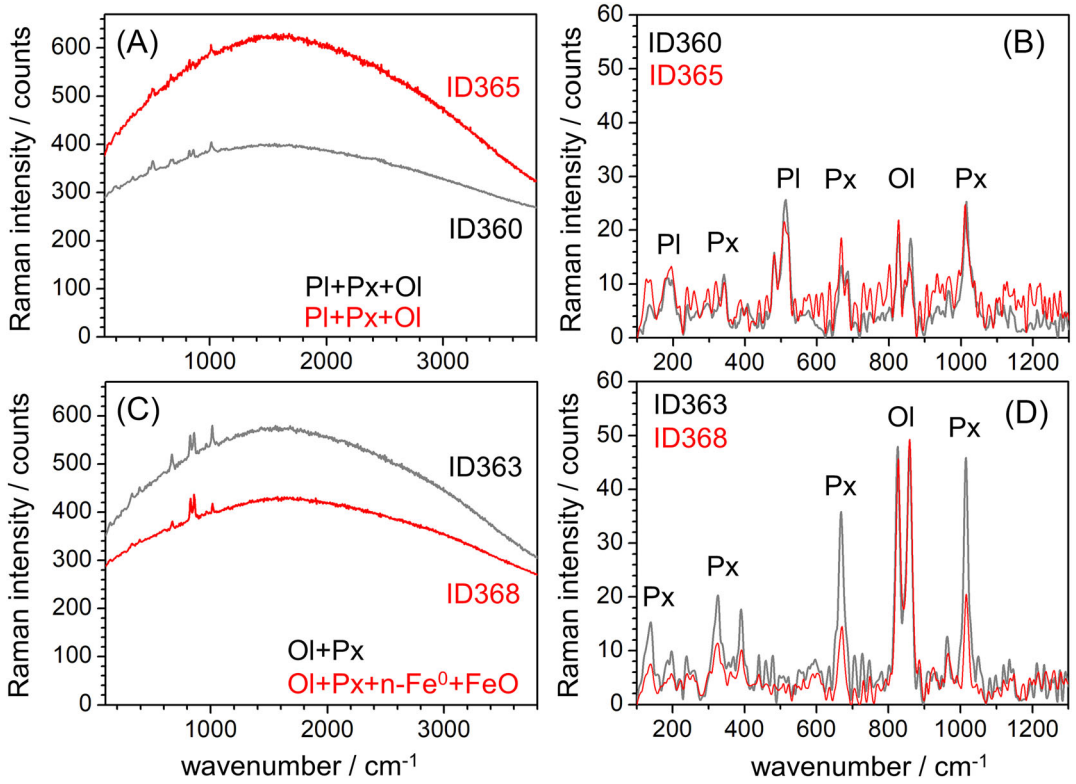

FIGURE 3 Averaged (2,500) Raman spectra of the non-irradiated (black) and irradiated (red) samples with the IDs 360/365 and IDs 363/368 taken at different locations. In black, the non-irradiated spectra show olivine, which can be identified by the typical Raman lines DP at 823/857 cm^{-1}; pyroxenes with their typical bands at 340, 391, 667/686, 1,012 and 1,014 cm^{-1}; and plagioclase with the Raman lines at 482 and 512 cm^{-1}. In red, the irradiated samples show the same Raman bands but with a higher PL for samples containing Plagioclase (Pl; IDs 360/365) and decreasing of PL in samples with Olivine and Pyroxene only (Ol, Px; IDs 363/368).

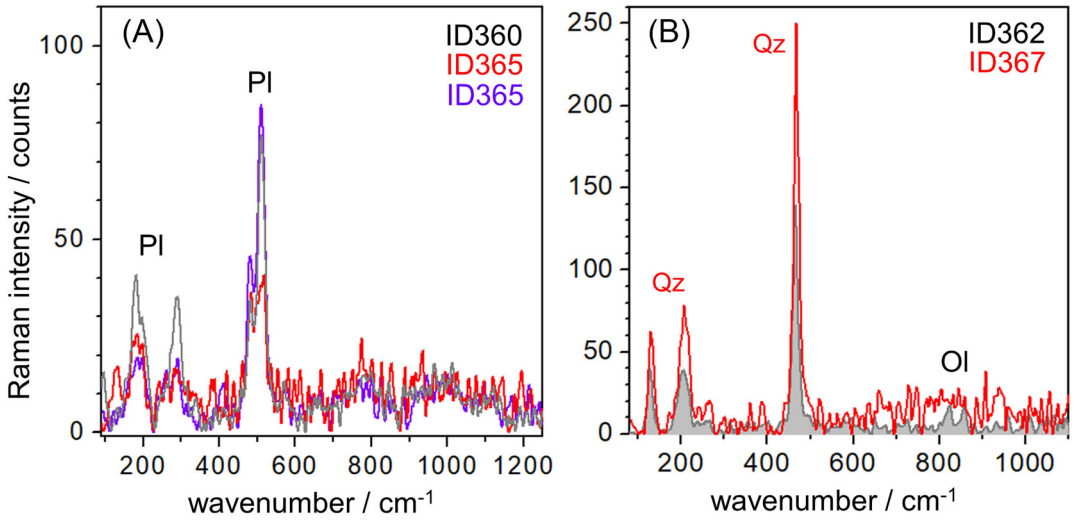

FIGURE 4 SW for the minerals with different melting temperatures as represented in single spectra of the original versus irradiated samples: (A) plagioclase in original (ID360) and irradiated (ID360/365) samples; (B) quartz in original (ID362) and irradiated (ID362/367) samples

mixed phases, before and after irradiation. The Raman spectra of the non-irradiated samples in the range from 200 to 1,200 cm^{-1} mainly exhibit the strongest Raman lines of the minerals contained in the pellets. Mineral mixtures result consequently in mixture spectra of at least two phases. The areas with dominating olivine,

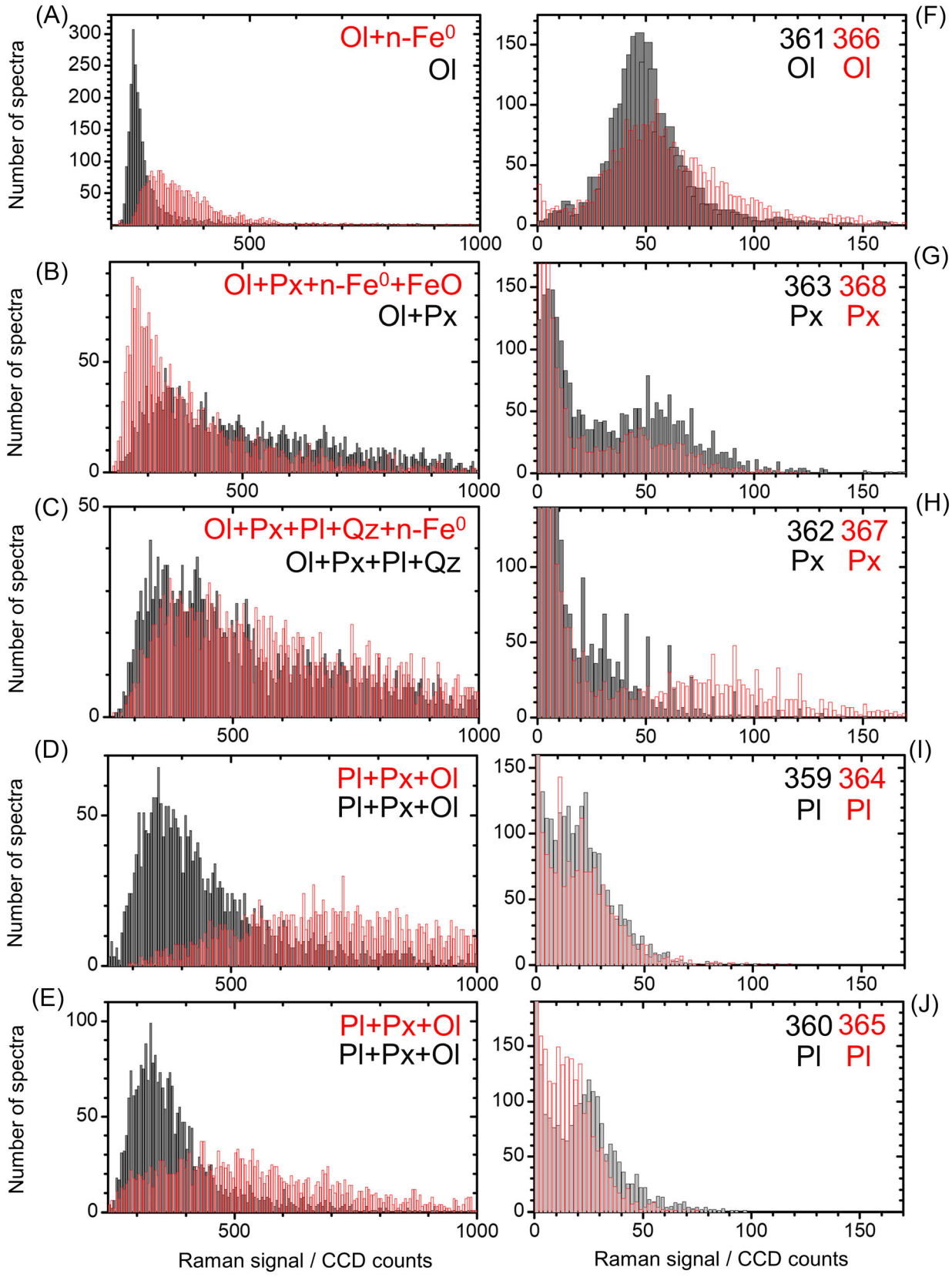

FIGURE 5 The histograms of the original non-irradiated (black) and irradiated (red) samples as mixtures with pyroxene, olivine and plagioclase as well as quartz as a minor phase: (A–E) PL signals; (F–J) Raman signatures of the mineral phases underwent strongest alteration

pyroxene and plagioclase phases remain clearly identified after irradiation by their strongest characteristic bands. However, diagnostic mineral peaks are less intense in mixtures after irradiation. The Si-O stretching modes in olivine, symmetric and anti-symmetric $A_g(\nu_1 + \nu_3)$ modes centred at about 823 and 857 cm^{-1} (DP feature), as well as the weaker stretching modes $A_g(\nu_3)$ at about 963 cm^{-1} and $B_{3g}(\nu_3)$ at about 921 cm^{-1} (the mode assignment as in Chopelas[24]) remain unchanged after irradiation, within the spectrometer resolution (Figure 3).

Also, the phonon modes in the pyroxene and plagioclase phases hold, in general, their characteristic energies. The characteristic modes of enstatite: M-O stretch at about 236 cm^{-1} (ν_1) and 340 cm^{-1} (ν_3), Si-O-Si bend at about 667 cm^{-1} (ν_{11}) and 686 cm^{-1} (ν_{12}) and Si-O_{br} stretch (O_{br} is a bridging oxygen) at about 1,012 cm^{-1} (ν_{16}) and 1,030 cm^{-1} (ν_{17}), and the modes of diopside: M-O stretch at about 230 cm^{-1} (ν_1), 325 cm^{-1} (ν_3) and Mg-O stretch at about 391 cm^{-1} (ν_4) (the mode assignment as in Huang et al.,[25] Mernagh[26] and Buzgar et al.[27]) are detectable in the irradiated samples.

The characteristic for feldspar minerals double peaks at about 482 and 512 cm^{-1} attributed to the T-O-T symmetric stretching modes of the four-member TO_4 tetrahedral ring where T = {Si;Al}[34] prevails in the spectra of the irradiated samples containing plagioclase (Figure 3). Its intensity degrades in the altered samples, however, significantly, and this mineral phase might be not detected commonly.

Both the PL signals and the Raman properties of the mineral phases show multidirectional evolution under simulated SW (Figures 3 and 5).

Alteration of different mineral phases is a matter of its melting temperature, enthalpy of fusion and local morphology, including surface roughness and neighbour grains.

Mineral phases with high melting temperature, such as quartz (Figure 4b) and olivine, tend to sustain their crystalline origin. The alteration of Raman line intensity of these phases is governed to large extent by overall conditions of Raman scattering: larger at Raman scattering enhancement (Figure 4B, Qz) or weaker when Raman scattering is reduced due to thin film deposits of ablated products. In contrast, amorphization of a mineral phase due to melting-related processes causes, as a rule, reduction of the Raman signatures: case of plagioclase (Figure 4A, Pl). All characteristic spectra, acquired for different mineral phases in the original samples, have been also measured in the samples after irradiation.

Contrary to the Raman line's positions, the PL, present in almost all spectra, is affected by this irradiation. In Figure 5, it can be seen that after irradiation, the PL intensity increases for the pellets with a dominant plagioclase content but also in the pellet with a plagioclase content of 11 wt.%. In contrast to the Pl-containing samples, the RS also increases after irradiation in the samples with Ol, but to a lesser extent than the PL.

In order to evaluate the PL evolution in the altered samples, we build the histograms of the evaluated PL signal derived in the spectral range beyond the characteristic Raman bands of the abundant minerals, at 1,600 cm^{-1}. The broad-band background signal in the row Raman spectrum includes the instrument-specific, nearly constant dark current signal (DC) and the sample-dependent PL signal.

The number of bins (columns) of every PL histogram is equal to 50 counts, bins of Raman signatures—two counts. Comparative PL histograms (Figure 5) of non-irradiated and irradiated samples show this systematic effect. For example, the highest PL values of all 2,500 spectra of the irradiated samples rich in plagioclase (IDs 359 360 362) are increased in comparison with the total PL of all spectra of an original sample. The histograms in Figure 5 show the distribution of background intensity, represented by CCD counts on the abscissa, obtained from 2,500 spectra at 50 × 50 points of each sample.

Figure 6 shows new mineral phases formed from the products of decomposition of original minerals and altered by the gas/volatiles (oxygen and carbon), which were apparently embedded in the original matrices or due to alteration after a break of vacuum in the chamber.

Another important finding is the detection of iron oxide phases: wüstite ($Fe^{2+}O$)[35] and maghemite (γ-Fe_2O_3)[36] very likely as nano-phases in the pellet ID 368 (Figure 6A). This proves the existence of a np-Fe^0 originated during the irradiation process and/or a fast alteration right after the simulated bombardment, although it seems to be weathered or oxidized already.[15,30]

Furthermore, a single spectrum of quartz phase was identified based on its typical, intense Raman peak at about 467 cm^{-1} (A_1 symmetric Si-O-Si stretching mode[27]) (Figure 6B), although its content is only 3 wt.% in the pellets with ID 362/367.

And to emphasize once again the accuracy of a Raman spectrometer, the measurement of siderite (Sd in Figure 6B) in the pellet with ID 363 (Raman Stoke 320 cm^{-1},[35] Figure 6), which presumably formed from the olivine due to the presence of trapped CO_2[37] in the pores of the pellets, is worth mentioning.

4 | DISCUSSION

With the establishment of Raman spectroscopy on space mission landers, for example, for the study of the Martian

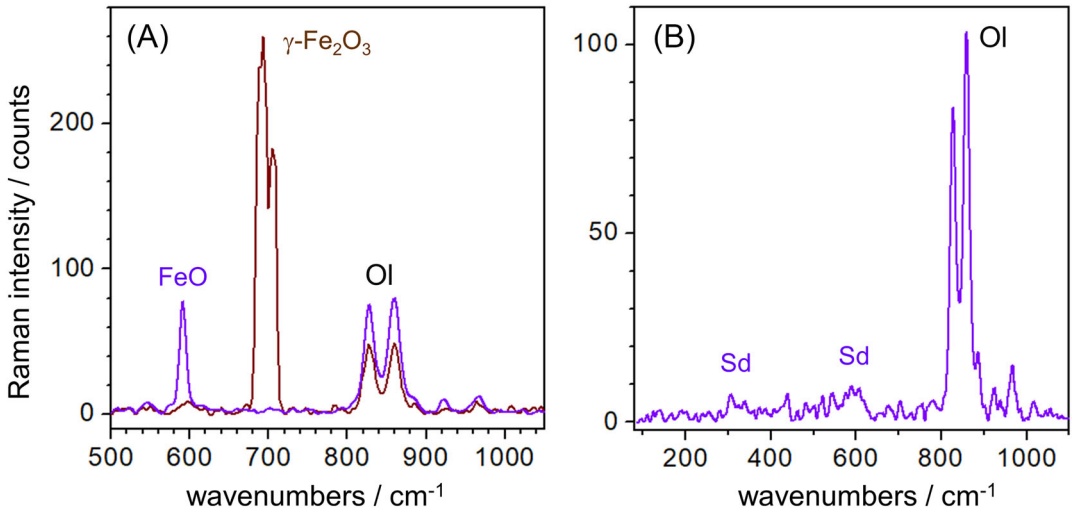

FIGURE 6 Mineral phases—products of alteration due to decomposition of original minerals. (A) Iron oxides in the Raman spectra of the irradiated sample (ID 368). Wüstite (purple) with its typical band centred peak[30] at about 590 cm^{-1} and maghemite[31] (brownish) with the typical band centred DB at around 700 cm^{-1} (693/706 cm^{-1}) can be identified in the spectra of the pellet with the ID 368. In both spectra, also, olivine is detected by the typical DP at 826/857 cm^{-1}. (B) Spectral features of amorphous-like siderite (bands around 320 and 595 cm^{-1})[30] in the Raman spectrum of the irradiated sample (ID 368)

surface and its moon Phobos, it is becoming increasingly important to perform appropriate laboratory studies. Ideally, analogue materials are used for this research, which are comparable to the target planet. For our study, we used natural rock-forming silicates from Earth, which are also expected to be present in various abundances on most planetary bodies, as well as on Phobos.[38] Due to their natural origin, the minerals are not pure and thus come even closer to the desired conditions. Moreover, in terms of possible experiments, it is important to think about scenarios that could have occurred before the time of landing on the surface of the body under study. Especially, bodies that lack a protective atmosphere have been committed to SW since their formation. As one possible source of SW, we investigated the continuous micrometeorite impacts simulated by laser irradiation.

As a result of our study and also as it is known from previous investigations,[39,40] a distinct surface darkening can be confirmed for the olivine- and pyroxene-containing pellets in the craters left in the irradiated areas. In contrast to this, the plagioclase-rich pellets show only laser-induced in parts amorphized impact craters. An explanation for the distinct darkening of the surfaces is the formation of np-Fe^0 in the minerals with abundant Fe within the mineral structure like—in the olivine (up to 10 g/mol) and lesser in the pyroxene mixes (around 4 g/mol). A lack of a np-Fe^0 in the laser irradiated plagioclase, which is nearly a Fe-free, was already assumed by infrared spectra as well as SEM and TEM analyses.[41] The SEM images of the original non-irradiated and irradiated pellets approve these suggestions. The pellets with olivine and pyroxene exhibit iron spherules with the sizes up to 3 μm as well as partial melting, whereas the plagioclase-rich samples show 'only' localized melting on the pellet surfaces. However, since the laser spot with a size of about 300 × 800 μm^2 is larger than the largest mineral grain present with 125 μm, the glassy layer may be wider than the original grain size.

Clear darkening and partial melting of ejected and the ablated material in the formed craters can be explained by a local impact heating due to laser irradiation—equal to micrometeorite bombardment. According to the earlier[9,30] and investigations by Loeffler et al.[32] with a comparable experimental setup, it is to be expected that a very thin small part of the surface melts for a short time, clumps and recrystallizes directly. During this fast and local heating process, nanophase Fe decomposed in situ from olivine and pyroxene in relation to the instantaneous (assuming that the heating is caused by a sub-pico-second energy transfer due to the short-living phonons) temperature rise. However, the Raman spectra of the altered samples still show the typical Raman peaks for these two minerals. This is consistent with the former TEM studies in which the np-Fe^0 is surrounded by an approximately 100 nm thick glassy material,[21,30,42] which consists of the former silicate. Below these space-weathered amorphous layers, the original silicates are still present and unchanged in their crystallinity, reflecting the characteristic modes in their Raman spectra. Compared to the iron bearing silicates, plagioclase has a much lower melting point; therefore,

the melting process is much more pronounced and goes deeper into the material. This is visible not only in the SEM images but also in the resulting Raman spectra. Following the investigation of Daniel et al.[43] and Pittarello et al.,[44] plagioclase shows extensive amorphization in the Raman spectra. Based on this observation, a shock pressure induced by laser irradiation of 20 GPa in minimum can be suggested (e.g., Stöffler et al.[45] and references therein), although it is an extremely fast process in the nanosecond-scale. Furthermore, the optical properties of the shocked plagioclase alter at about this pressure value,[46] which cause higher transparency of the material that is consistent with the appearance of the pellets after irradiation. However, one should mention that in our case, the very contrasting absorption efficiencies of the UV photons should kept in mind for the melting of plagioclase[47] in contrast to other silicates.[48]

In addition, it is likely that during the treatment, the single grains in the lasered area clump together at the surface due to the irradiation and—in case of olivine and pyroxene—an extremely thin nm or—in case of plagioclase—a thicker layer remains in glassy structure after irradiation. This can also be related to the penetration depth of the Raman laser and the resulting spectra. The penetration depth of Raman spectroscopy is dependent on the wavelength used and the mineral investigated.[49]

For the investigated silicates, it should be several μm, which is consistent with the observed Raman spectra. The plagioclase-rich areas show a glassy-like (spectrally broadened bands) spectrum consisting with surface amorphization. However, the amorphous plagioclase is difficult to detect due to the irradiation. Concerning the other main minerals—olivine and pyroxene—the Raman spectra itself exhibit a lower intensity, which most likely can be explained with a thin glassy layer around these minerals as remnants of the irradiation. Such glassy layers are also found in the regolith on the Moon as well as on the Itokawa asteroid (Qafoku et al.[37] and references therein).

A weaker magnitude of the characteristic optical absorption bands was also found in the evaluation of the laboratory irradiated rock-forming silicates within UV/VIS and NIR spectra.[50,51] Additionally, this phenomenon has also been found in the analysis of real remote sensing data, which provided spectra with a rather low contrast of characteristic optical and infrared-active bands.[32,50] Here, the formation of a np-Fe^0 is used as a possible explanation for these darkening.[51] In our case, it is not clear whether the RS decrease comes from np-Fe^0 and/or the glassy layer.

In general, metal nanoparticles (NPs) are able to focus light into small volumes.[52] These effects arise from the excitation of plasmon resonances of the particles (commonly called as localized surface plasmon resonances [LSPRs]), which are coherent oscillations of their conduction electrons. The light-concentrating effects of metal NPs are a consequence of the enhanced electromagnetic fields that are generated by the LSPR. These external fields are amplified when two or more particles are brought into close proximity.

Moreover, to the differences in the individual Raman peaks and in the intensity of the spectra described above, we observed very different behaviour of the silicates' PL background after irradiation. The observed PL signals retrieve their characteristic spectra after irradiation, while their magnitude changes in different directions depending on content of original mineral mixes (Figures 3 and 5). The largest PL signals in our samples were recorded for natural pyroxenes, which is consistent with observation of background signals in Raman spectra of meteorites,[17] while the smallest PL was accompanying by spectra of natural olivine minerals. In contrast to the np-Fe^0 bearing silicates where the PL decreases after irradiation, plagioclase exhibits an increase. One possible explanation of such surface passivation, especially for olivine-pyroxene mixtures, was given in our former work.[9] And even though, in this work, the np-Fe^0 particles could not be resolved by Raman, the authors formulate the hypothesis that the PL is due to an excess of freely available electrons in the conduction band that relax to the vibrational or ground state upon excitation with the Raman laser. Upon precipitation of a free iron by a laser irradiation, some of these electrons will be bound by the Fe and will no longer be available for PL processes when Raman laser excitation occurs. Another explanation is that np-Fe^0 passivates PL atoms, such as rare-earth elements, if they are present in the mineral.[53] As a result, the PL level decreases for silicates with np-Fe^0 that is visible in a shift in the histograms (Figure 5) to lower Raman intensity values (in CCD counts) for irradiated samples compared to non-irradiated ones. However, compared to our former work, we cannot demonstrate that the overall PL values disappear on a nanophase bearing surfaces, but this may be related to the lower overall irradiance density of the pellet surface, because in the former measurements, we covered the whole surface with irradiation rectangles, which is not the case in the present study due to the known instability of plagioclase.[41]

Opposite to mixtures without plagioclase, in plagioclase containing mixtures, the background PL increases significantly. We assume that due to the irradiation process, the glassy surface thus produced allows increased light penetration, leading to an increase in the density of light-activated PL centres,[54] which could not be passivated by, for example, nanophase Fe.

And although in the present study the laser irradiation map did not cover the whole pellet, another trigger for PL might be the slightly rough surface of the non-irradiated pellets itself. The Raman laser is multiple scattered on a rough surface and is better focused on a flatter surface. This is the case for olivine and pyroxene, where a very thin and small part of the surface melts for a short time, agglutinates and recrystallizes directly by forming larger interconnected areas. Therefore, agglutination might reduce the PL in the areas where the irradiation rectangle is present and should kept in mind in measurements from space missions. Plagioclase loses its crystal symmetry by forming a diaplectic glass, and therefore, as a glass, its PL is not reduced.[55]

Finally, a really remarkable find is the detection of iron oxides: wüstite and maghemite, which prove the existence of np-Fe^0 by Raman scattering. We assume that iron oxidation is primarily a post-ablation process that takes place after the chamber with the irradiated sample has been opened to the atmosphere. At this moment, reactions with ambient atmosphere took place, and $Fe^{2+}O$ or γ-$Fe_2{}^{3+}O_3$ could arise. This scenario would agree the temperature evolution of unstable iron oxides as reported in.[56] However, we do not speculate if iron oxides could be formed already due to composition directly during and after ablation; however, point that while nano-maghemite is well known, nano-wüstite is unusual in such a physical process as it is not stable.[57]

And quartz particles and siderite could be identified during the measurements. That means Raman is also suitable to identify also trace or minor minerals in the mixture under a fast-scanning scenario, what demonstrates the suitability of Raman spectrometers on space missions.

5 | SUMMARY AND CONCLUSION

The aim of studying micrometeorite bombardment simulated by nanosecond-pulse laser irradiation is to investigate whether Raman spectroscopy is capable to follow alteration triggered by this special type of SW. During our investigations, we have seen that the behaviour of the material to the laser bombardment and thus also the spectra is extremely material or composition dependent. Following the penetration depth of the Raman signal, a 'fresh' or gardened surface is only distinguishable if the material was changed completely. The mineral phases with a simple chemistry/composition, such as quartz, are basically not altered 'chemically' and not producing the side products. In contrast, structural more complex iron-bearing mineral phases, such as olivine, can form nano-Fe^0 phase, which cause optical 'darkening' but also obviously the surface enhancement for Raman scattering. In addition, phases with a low melting temperature (plagioclase) undergo partial melting, while those with higher melting temperatures (pyroxenes) may undergo partial surface amorphization reflected in the spectral broadening of their Raman lines.

However, the studied body of the Solar System may have been entirely rearranged by SW since its formation, so that the space weathered surface might be buried underneath a fresher surface. If the PL is considered, this can be a sign for SW of olivine and pyroxene (decreasing) or plagioclase (increasing). Therefore, our results show that Raman spectroscopy is very capable of studying the surface of a planetary body. And, moreover, Raman spectroscopy is suitable for the detection of two or more even small minerals in only one measurement sequence.

ACKNOWLEDGEMENTS

The authors would like to thank U. Heitmann for sample preparation. Thanks also to the editor Philippe Colomban and three anonymous reviewers for providing very helpful reviews that greatly improved the manuscript. The laser irradiation experiments are supported by a grant 50 QW 1701 from the Deutsches Zentrum für Luft- und Raumfahrt. The Raman measurements are carried out at the joint Raman Spectroscopy Laboratory of the DLR Institutes of Planetary Research and Optical Sensor Systems in Berlin. Open Access funding enabled and organized by Projekt DEAL.

ORCID

Iris Weber https://orcid.org/0000-0001-7598-3951
Ute Böttger https://orcid.org/0000-0003-2266-7271
Maximilian P. Reitze https://orcid.org/0000-0002-7092-3404

REFERENCES

[1] K. H. Williford, K. A. Farley, K. M. Stack, A. C. Allwood, D. Beaty, L. W. Beegle, R. Bhartia, A. J. Brown, M. de la Torre Juarez, S.-E. Hamran, M. H. Hecht, J. A. Hurowitz, J. A. Rodriguez-Manfredi, S. Maurice, S. Milkovich, R. C. Wiens, *From the Habitability to Life on Mars* (Eds: N. A. Cabrol, E. A. Grin), Elsevier **2018**, Ch. 11 275.

[2] F. Rull, S. Maurice, I. Hutchinson, A. Moral, C. Perez, C. Diaz, M. Colombo, T. Belenguer, G. Lopez-Reyes, A. Sansano, O. Forni, Y. Parot, N. Striebig, S. Woodward, C. Howe, N. Tarcea, P. Rodriguez, L. Seoane, A. Santiago, J. A. Rodriguez-Prieto, J. Medina, P. Gallego, R. Canchal, P. Santamaría, G. Ramos, J. L. Vago, RLS Team, *Astrobiol.* **2017**, *17*, 627.

[3] Y. Cho, U. Böttger, F. Rull, H.-W. Hübers, T. Belenguer, A. Börner, M. Buder, Y. Bunduki, E. Dietz, T. Hagelschuer, S. Kameda, E. Kopp, M. Lieder, G. Lopez-Reyes, A. G. M. Inza, S. Mori, J. A. Ogura, C. Paproth, C. P. Canora, M. Pertenais, G. Peter, O. Prieto-Ballesteros, S. Rockstein, S. Rodd-Routley, P. R.

Perez, C. Ryan, P. Santamaria, T. Säuberlich, F. Schrandt, S. Schröder, C. Stangarone, S. Ulamec, T. Usui, I. Weber, K. Westerdorff, K. Yumoto, *Earth Planets Space* **2021**, *73*, 232.
[4] C. M. Pieters, S. Murchie, N. Thomas, D. Britt, *Planet. Sp. Sci.* **2014**, *102*, 144.
[5] U. Böttger, J.-P. de Vera, J. Fritz, I. Weber, H.-W. Hübers, D. Schulze-Makuch, *Planet. Sp. Sci.* **2012**, *60*(1), 356.
[6] I. Weber, U. Böttger, S. G. Pavlov, E. K. Jessberger, H. W. Hübers, *Planet. Sp. Sci.* **2014**, *104*(B), 163.
[7] A. Wang, R. L. Korotev, B. L. Jolliff, Z. Ling, *Planet. Sp. Sci.* **2015**, *112*, 23.
[8] M. Veneranda, G. Lopez-Reyes, J. A. Manrique-Martinez, A. Sanz-Arranz, E. Lalla, M. Konstantinidis, A. Moral, J. Medina, F. Rull, *Nat. Res. Sci. Rep.* **2020**, *10*, 16954.
[9] I. Weber, U. Böttger, F. Hanke, M. P. Reitze, M. Heeger, T. Adolphs, H. F. Arlinghaus, *J. Raman Spectrosc.* **2022**, *53*, 411.
[10] A. Morlok, C. Renggli, B. Charlier, O. Namur, S. Klemme, M. P. Reitze, I. Weber, A. Stojic, K. E. Bauch, H. Hiesinger, H. Helbert, *Icarus* **2023**, *396*, 115498.
[11] C. J. Bennett, C. Pirim, T. M. Orlando, *Chem. Rev.* **2013**, *113*, 9086.
[12] C. M. Pieters, L. A. Taylor, S. K. Noble, L. P. Keller, B. Hapke, R. V. Morris, C. C. Allen, D. S. McKay, S. Wentworth, *Meteorit. Planet. Sci.* **2000**, *35*, 1101.
[13] B. Hapke, *J. Geophys. Res.* **2001**, *106*, 39.
[14] C. M. Pieters, S. K. Noble, *J. Geoph. Res.: Planets* **1865**, *2016*, 121.
[15] I. Weber, M. P. Reitze, A. Morlok, A. N. Stojic, H. Hiesinger, N. Schmedemann, K. E. Bauch, J. H. Pasckert, J. Helbert, *Icarus* **2023**, *404*, 115683.
[16] L. Nasdala, D. C. Smith, R. Kaindl, M. A. Ziemann, *Earth Syst. Sci. Data* **2021**, *13*, 4465.
[17] A. Wang, J. Wei, R. L. Korotev, *J. Raman Spectr.* **2020**, *51*, 1636.
[18] F. Sedaghatpour, D. W. G. Sears, *Meteor. Planet. Sci.* **2009**, *44*, 653.
[19] Z. C. Ling, A. Wang, B. L. Jolliff, *Icarus* **2011**, *211*, 101.
[20] U. Böttger, M. Maiwald, F. Hanke, M. Braune, S. G. Pavlov, S. Schröder, I. Weber, H. Busemann, B. Sumpf, G. Tränkle, H.-W. Hübers, *Planet. Space Sci.* **2017**, *144*, 106.
[21] I. Weber, A. N. Stojic, A. Morlok, M. P. Reitze, K. Markus, H. Hiesinger, S. G. Pavlov, R. Wirth, A. Schreiber, M. Sohn, H. W. Hübers, J. Helbert, *Earth Planet. Sci. Lett.* **2020**, *530*, 115884.
[22] R. Brunetto, T. Pino, E. Darois, A.-T. Cao, L. d'Hendecourt, G. Strazulla, P. Bréchignac, *Icarus* **2009**, *200*, 323.
[23] M. Matsuoka, T. Nakamuara, T. Hiroi, S. Okumura, S. Sasaki, *Astrophys. J. Let.* **2020**, *890*(L23), 12.
[24] A. Chopelas, *Am. Mineral.* **1991**, *76*, 1101.
[25] E. Huang, C. H. Chen, T. Huang, E. H. Lin, J. A. Xu, *Am. Mineral.* **2000**, *85*, 473.
[26] T. P. Mernagh, *J. Raman Spec.* **1991**, *22*, 453457.
[27] N. Buzgar, A. I. Apopei, V. Diaconu, A. Buzatu, *Iasi Seria Geologie* **2013**, *59*(1), 5.
[28] M. P. Reitze, I. Weber, H. Kroll, A. Morlok, H. Hiesinger, K. E. Bauch, A. N. Stojic, J. Helbert, *Earth Planet. Sci. Lett.* **2021**, *554*, 116697.
[29] D. S. McKay, R. M. Fruland, G. H. Heiken, *Geochim. Cosmochim. Acta* **1974**, *1*, 887.
[30] A. N. Stojic, I. Weber, A. Morlok, S. G. Pavlov, H. Hiesinger, M. P. Reitze, A. Maturilli, N. Schmedemann, K. E. Bauch, J. H. Pasckert, J. Helbert, *Icarus* **2023**, *391*, 115344.
[31] J. Alsemgeest, S. G. Pavlov, U. Böttger, I. Weber, *ACS Earth Space Chem.* **2022**, *6*, 2167.
[32] M. J. Loeffler, C. A. Dukes, R. Christoffersen, R. A. Baragiola, *Meteorit. Planet. Sci.* **2016**, *51*(2), 261.
[33] J. J. Papike, S. B. Simon, J. C. Laul, *Rev. Geophys.* **1982**, *20*(4), 761.
[34] S. K. Sharma, S. M. Angel, M. Ghosh, H. W. Hubble, P. G. Lucey, *Appl. Spectros.* **2002**, *56*(6), 699.
[35] M. Hanesch, *Geophys. J. Int.* **2009**, *177*(3), 941.
[36] C. Hartmann, M. Elsner, R. Niessner, N. P. Ivleva, *Appl. Spectrosc.* **2020**, *74*(2), 193.
[37] O. Qafoku, L. Kovarik, R. K. Kukkadapu, E. S. Ilton, B. W. Arey, J. Tucek, A. R. Felmy, *Chem. Geol.* **2012**, *332*, 124.
[38] G. Poggiali, M. Matsuoka, M. A. Barucci, J. R. Brucato, P. Beck, S. Fornasier, A. Doressoundiram, F. Merlin, A. Alberini, *Astronom. Soc.* **2022**, *516*(1), 465.
[39] S. Sasaki, T. Hiroi, K. Nakamura, Y. Hamabe, E. Kurahashi, M. Yamada, *Adv. Space Res.* **2002**, *29*(5), 783.
[40] J. Xu, B. Mo, Y. Wu, Y. Y. S. Zhao, H. Lin, B. Ye, J. Michalski, Y. Li, K. Tai, C. Li, Z. Guo, C. Qi, S. Liu, X. Li, J. Liu, *Astronom. Astrophys.* **2023**, *672*, A115.
[41] L. V. Moroz, L. V. Starukhina, S. S. Rout, S. Sasaki, J. Helbert, D. Baither, A. Bischoff, H. Hiesinger, *Icarus* **2014**, *235*, 187.
[42] S. Sasaki, E. Kurahashi, C. Yamanaka, K. Nakamura, *Adv. Space Res.* **2003**, *31*(12), 2537.
[43] I. Daniel, P. Gillet, P. F. McMillan, G. Wolf, M. A. Verhelst, *J. Geophys. Res.: Solid Earth.* **1997**, *102*(B5), 10313.
[44] L. Pittarello, J. Fritz, J. Roszjar, C. Lenz, C. Chanmuang, N. C. Koeberl, *Maps* **2020**, *3*, 669.
[45] D. Stöffler, C. Hamann, K. Metzler, *Maps* **2018**, *53*(1), 5.
[46] J. Fritz, V. Assis Fernandes, A. Greshake, A. Holzwarth, U. Böttger, *Maps* **2019**, *54*(7), 1533.
[47] A. E. R. Malins, N. R. J. Poolton, F. M. Quinn, O. Johnsen, P. M. Denby, *J. Phys. D: Appl. Phys.* **2004**, *37*, 1439.
[48] M. Legesse, H. Park, F. ElMellouhi, S. N. Rashkeev, S. Kais, F. H. Alharbi, *ChemPhysChem* **2018**, *19*(8), 892.
[49] J. J. Song, C. Yang, H. Y. Hu, X. Y. Dai, D. Wang, H. M. Zhang, *Phys. Mechan. Astron.* **2013**, *56*(11), 2065.
[50] K. L. Donaldson Hanna, L. C. Cheek, C. M. Pieters, J. F. Mustard, B. T. Greenhagen, I. R. Thomas, N. E. Bowles, *J. Geophys. Res.: Planets* **2014**, *119*, 1516.
[51] P. G. Lucey, M. A. Riner, *Icarus* **2011**, *212*, 451.
[52] G. V. Hartland, L. V. Besteir, P. Johns, A. O. Govorov, *ACS Energy Lett.* **2017**, *2*(7), 1641.
[53] V. Fuertes, J. F. Fernández, E. Enríquez, *Optica* **2019**, *6*(5), 668.
[54] H. Chen, R. W. Stimets, *Am. Mineral.* **2014**, *99*(2–3), 332.
[55] F. Hanke, B. J. A. Mooij, F. Ariese, U. Böttger, *J. Raman Spec.* **2019**, *50*(7), 969.
[56] D. L. de Faria, S. V. Silva, M. T. de Oliveira, *J. Raman Spectr.* **1997**, *28*, 873.
[57] M. Yin, Z. Chen, B. Deegan, S. O'Brien, *J. Materials Res.* **1987**, *2007*, 22.

How to cite this article: I. Weber, S. G. Pavlov, U. Böttger, M. P. Reitze, *J Raman Spectrosc* **2024**, *55*(8), 901. https://doi.org/10.1002/jrs.6676